J. Phys. D: Appl. Phys. **29** (1996) 1751–1760. Printed in the UK

Interband electronic structure of a near-Σ11 grain boundary in α-alumina determined by spatially resolved valence electron energy-loss spectroscopy

Harald Müllejans† and Roger H French‡

† Max-Planck-Institut für Metallforschung, Institut für Werkstoffwissenschaft, Seestraße 92, D-70174 Stuttgart, Germany
‡ DuPont Corporation Central Research and Development, E356-323, Experimental Station, Wilmington, Delaware 19880-0356, USA

Received 14 August 1995, in final form 2 January 1996

Abstract. Valence electron energy-loss spectroscopy in a dedicated scanning transmission electron microscope has been used to obtain the interband transition strength of bulk α-Al_2O_3. The interband electronic structure was obtained from critical point modelling. Comparison to established results from vacuum ultraviolet spectroscopy was used to improve the analysis of the energy-loss spectra and quantitative agreement between both methods was obtained. Spatially resolved measurements of a near-Σ11 tilt grain boundary in α-Al_2O_3 were analysed with the same procedure. This revealed an increase in the electron occupancy of the O 2p valence band to conduction band transitions which can be associated with an increased ionic character of the bonding at the grain boundary with respect to the bulk material. This is consistent with the results of other studies which determined the atomic structure and then calculated the electronic band structure of the same near-Σ11 tilt grain boundary. Quantitative analysis of valence electron energy-loss spectroscopy can be regarded as a new electronic structure tool for application to localized structures such as internal interfaces in our quest to better understand their micro- and macroscopic properties.

1. Introduction

The optical properties of insulators are a direct probe of the interband transitions and valence electronic structure and are therefore currently of great interest. Our work is devoted to understanding the localized electronic structure of internal interfaces using both experimental and theoretical methods. From a basis in interband optical properties it is possible to measure various observables, such as the optical reflectance or the electron energy loss, or calculate the imaginary part of the dielectric function. Because the real and imaginary parts of the complex optical properties are related to each other by causality relations it is possible to calculate the corresponding part with the help of a Kramers Kronig (KK) dispersion analysis. It is then possible to deduce any other of the complex optical properties from a knowledge of the real or imaginary component of any one optical property [1]. Therefore in order to compare the results of different measurements and methods, such as vacuum ultraviolet (VUV) spectroscopy and spatially resolved valence electron energy-loss spectroscopy (SR VEELS) we need only to improve our KK analysis of the experimental observables. Typically this will require a careful understanding of the nature and properties of the signals, noise and artifacts present in the data, so as to be alert for analytical anomalies while processing the information.

The optical properties are closely related to the electronic structure of the material, in particular the interband transitions between the occupied valence band and the empty conduction band. Traditionally the dielectric function $\varepsilon = \varepsilon_1 + i\varepsilon_2$ is taken as the common optical property used for comparison between various methods. However, for quantitative analysis of the electronic structure it is desirable to use the interband transition strength J_{CV}, which is just an energy weighted function of the dielectric constant (see definition in equation (1)). The interband transition strength is preferred because it is closely related to the joint density of states, with the interband matrix elements considered. The interband

critical points demonstrate their appropriate topological line shapes in J_{CV}, which is not the case for the dielectric constant [2].

Reflectivity measurements in VUV spectroscopy have been used recently to obtain the interband transition strength of various insulators, in particular α-Al_2O_3 [3–5] and AlN [6, 7]. With critical point modelling it is then possible to obtain quantitative information on the electronic structure [2]. For example this method has been used to follow the effects of the electron phonon interaction in the electronic structure of α-Al_2O_3 up to the melting point, where strong anharmonicity is observed [5]. Another interesting application in materials science is the calculation of the van der Waals attraction forces of wetted interfaces directly from the interband transition strengths of the component materials using quantum field theory results [8]. One drawback of the VUV optical method is its limited spatial resolution. Measurements are restricted to macroscopic single crystals or polycrystals. In the latter case the data are automatically averaged over all different orientations. It is impossible to obtain information directly from localized defects in the material such as grain boundaries. It is generally accepted, however, that in many cases the grain boundaries are decisive for the macroscopic properties. Furthermore in the case of thin intergranular films, such as present in Si_3N_4 for example, VUV spectroscopy cannot determine the Hamaker constant unless a reference material with exactly the same composition as present in the grain boundary film is provided [9]. It is virtually impossible to manufacture such a reference material due to the complicated and incompletely understood segregation effects occurring during the processing of Si_3N_4.

These drawbacks can only be overcome by a method which offers high spatial resolution and therefore the direct investigation of interfaces and intergranular films on a nanometre scale. Such a method is SR VEELS. The theory of inelastic electron scattering shows that the electron energy-loss (EEL) spectra are proportional to $\mathrm{Im}(-1/\varepsilon)$ where ε is the dielectric function [10]. Therefore EEL spectra can be analysed to give the complex optical properties and in particular the interband transition strength for a material. Then critical point modelling as developed for VUV spectroscopy can be applied. In the past, however, only the dielectric function ε has been calculated from the measured EEL spectra and the application was limited to bulk materials. Dielectric theory has been used to calculate the expected EEL signal for special geometries and has shown good agreement with experiment [11, 12]. In these cases the spatial resolution available in a dedicated scanning transmission electron microscope (STEM) has been used to obtain spectra with an electron beam diameter of 1 nm or less. However, the possibility of quantitatively analysing the EEL spectra to produce detailed electronic structure information in combination with high spatial resolution has not been attempted. With these same analytical methods it will also become possible to measure Hamaker constants *in situ* [9].

This paper shows the development of a new method for bulk material and the application to a model grain boundary. First we refine our VEELS data analysis by quantitative comparison of VEELS results for bulk α-Al_2O_3 with results obtained using VUV spectroscopy from single crystals. Taking the well established results from VUV as a reference it was possible to optimize the VEELS data analysis to obtain *quantitative* agreement. Then VEELS was obtained from a near-$\Sigma 11$ tilt grain boundary (GB) in α-Al_2O_3. This served as a model GB and was chosen since it has been extensively studied by other methods. High-resolution transmission electron microscopy (HRTEM) [13] in conjunction with static lattice calculations of the GB structure [14] has provided information on the atomic structure of the GB. Furthermore the electron energy-loss near-edge structures (ELNES) has been measured from the GB atoms and interpreted with respect to the coordination and bond length of the atoms at the GB [15]. All this structural information was found to be mutually consistent. Based on the structural data there has been recently an effort to calculate the electronic band structure [16] and optical properties [17] of this GB from first principles. The experimental results presented here will be discussed in relation to these other investigations.

Some preliminary results have been presented before [18, 19], but data analysis continues to improve. In this paper we present our current understanding and analysis capability for VEELS. This shows that VEELS could be a useful method to determine the electronic structure of internal interfaces.

2. Experiment

2.1. Sample

The same cross sectional TEM specimen previously prepared for and examined by HRTEM [13] and the ELNES [15] measurements was used in this study. The near-$\Sigma 11$ bicrystal was melt grown using two seed crystals which had been purified by multiple zone refinement [20]. The cation impurity level was less than 38 ppm and the total impurity level below 59 ppm as determined by SIMS. The cross sectional TEM specimens had originally been coated with a thin carbon film to avoid charging in the HRTEM investigation. For the experiments performed here it was found that this was not necessary and the carbon layer was removed by a short ion beam thinning.

2.2. Data acquisition

The VEELS measurements were acquired with a parallel electron energy-loss spectrometer (PEELS) (Gatan 666) fitted to a dedicated STEM (Vacuum Generators HB501) operating at 100 keV. The spectrometer consists of a magnetic prism, quadrupole lenses and a photodiode array for parallel recording. The microscope is equipped with a high-resolution pole piece and a cold field emission electron source. The system has an energy resolution of 0.7 eV, determined by the full-width-half-maximum of the zero loss peak. The beam was focused to give less than 1 nm diameter. The convergence and collection semi-angle were both 7 mrad. Spectra were acquired while the beam was scanning an area of 3 nm $\times$ 4 nm. An image of the

investigated specimen area was simultaneously observed in the high-angle annular dark field detector and specimen drift was corrected manually with the beam shift coils. This acquisition mode sacrifices spatial resolution and sensitivity to the GB. At the time the experiments were performed it was not possible to acquire several spectra with different acquisiton times (see below) from the same area. Only recent improvements in hardware and software permit this mode of operation which allows one-dimensional profiles across the GB where the irradiated area is identical to the profile of the primary electron beam. This will be used in future work. Visual inspection of the image before, during and after data acquisition did not show any sign of electron beam irradiation damage of the specimen.

To increase the dynamic range of the detector a set of three spectra was acquired at each position, with a total spectral width of 50 eV each. Between the spectra the acquisition time and the energy range was varied to obtain unsaturated statistically relevant data for the Al–L edge (79 eV), the bulk plasmon loss (25 eV) and the zero loss (0 eV) respectively. Four sets of spectra were taken, two while the beam was scanning an area centrally located on the GB and two while scanning over bulk material near the GB. All spectra were corrected for readout pattern and dark current and then the spectra in each set were spliced together to give one continuous spectrum in the energy loss range -10 to 80 eV. The data acquisition at each area took about thirty seconds and the whole measurement of one data set was performed in less than two minutes.

2.3. Data analysis

The data acquisition and analysis was performed on personal computers. The PEELS is controlled by a Macintosh computer and the dark current and gain correction, splicing and single scattering deconvolution were done on this platform under EL/P†. The other analysis was performed on an IBM compatible 486 PC under GRAMS‡. Various routines have been implemented for single scattering deconvolution (SSD), Kramers Kronig (KK) analysis, critical point (CP) modelling and Hamaker constant calculations§.

3. Results

3.1. Methods of VEELS data analysis

The two spectra from the bulk grains were first used to optimize the data analysis of the VEELS spectra taking the results from VUV spectroscopy as a reference. This comparison was performed at all stages of the analysis procedure.

† EL/P is a software package for acquiring and processing EEL spectra from the PEELS system. It is available from Gatan Incorporated, 6678 Owens Drive, Pleasanton, CA 94566, USA.

‡ Grams/386 is a 32-bit PC-based spectroscopy environment which supplies a vectorized programming language, three-dimensional relational databases and is the environment in which the Hamaker.ab program has been developed. Grams/386 is available from Galactic Industries, 325 Main Street, Salem, NH 03079, USA.

§ Veels.ab, KKDupont.ab, Critpt.ab and Hamaker.ab are available from Spectrum Squared, 755 Snyder Hill Road, Ithaca, NY 14850, USA.

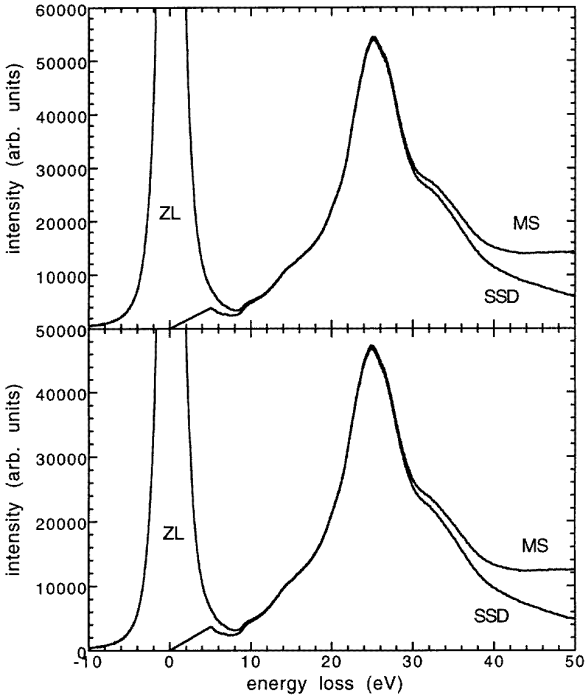

Figure 1. Two examples of as-acquired SR VEELS spectra of α-Al_2O_3, with the zero loss (ZL) and multiple scattering (MS) present, and the single scattering deconvoluted (SSD) results obtained using the Gatan routines. Notice the artificial shape where the ZL peak is truncated at 5 eV and also the intensity present below the 8.8 eV band gap even after SSD: the shape of the SSD spectrum determined using these methods is not asymptotic to zero below the band gap.

3.1.1. Single scattering deconvolution. Figure 1 shows the EEL spectrum from bulk α-Al_2O_3 obtained after splicing. Multiple scattering was removed from the recorded VEELS by a Fourier-log deconvolution of the entire spectrum [10]. The routine employed in the EL/P software integrates the intensity of the zero loss up to the first minimum and replaces it with a delta function [10]. This is a crude approximation and finite intensities remained in the band-gap region which are not meaningful and indicate incomplete data correction. It is found experimentally that a zero loss recorded through a hole (i.e. with no inelastic scattering present in the spectrum) has wings which extend to several tens of electronvolts, basically over the whole detector array.

Currently we try to solve this in two different ways, with curve fitting of analytical functions (e.g. a Lorentzian) or experimental zero loss line shapes (recorded shortly before or after the experiment with the same settings of the microscope and spectrometer while the beam is passing through a hole in the specimen) to the right-hand wing of the zero loss peak within the known band-gap region (for α-Al_2O_3 the band gap is larger than 8.8 eV at room temperature [3]). Both methods have wings which extend over the full spectral range and are therefore suitable. It is known, however, that the line shape of the zero loss cannot be described fully by an analytical function. Likewise the experimentally recorded line shape is missing some effects

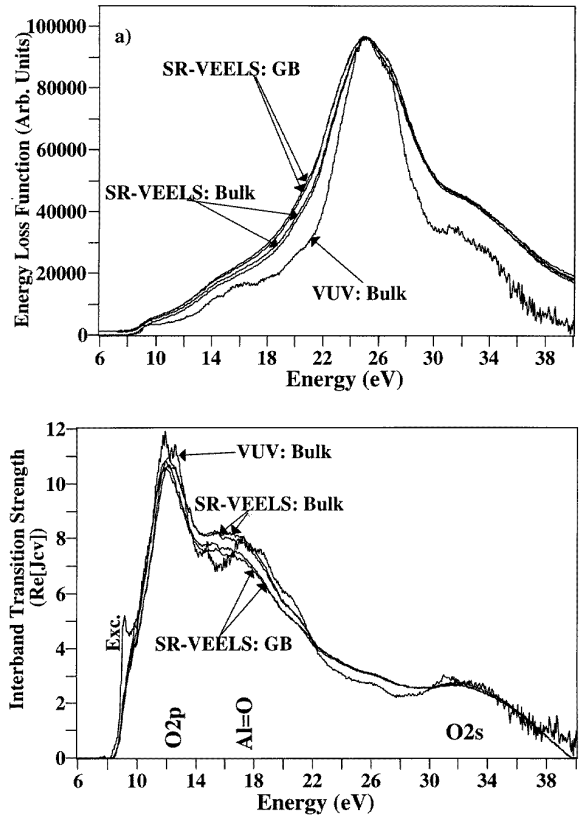

Figure 2. (*a*) Single scattering deconvoluted STEM VEELS spectra for two locations in Grain 1 and 2 and two locations along the near-Σ11 tilt grain boundary compared with VUV EELS spectra and (*b*) the interband transition strength (in eV^2) determined by Kramers Kronig analysis of these VEELS spectra compared with those determined by Kramers Kronig analysis of VUV reflectance spectra.

such as phonon scattering [10] which is present in the actual spectrum but should preferably be removed since it is not related to the dielectric function.

At the time the experiment was carried out this complication had not been realized fully and no experimental line shapes were recorded. Therefore we fitted a power law to the remaining intensities in the band-gap region and subtracted it over the entire spectral range. A remaining constant offset on the spectrum was also removed. Figure 2(*a*) shows the results of these baseline-subtracted multiple scattering corrected VEEL spectra compared to the VEEL spectrum directly calculated from VUV data. From the VEEL spectra the absolute specimen thickness and the mean free path for inelastic scattering can be calculated [10]. For the four data sets the thickness was 80 ± 2 nm and the mean free path 112 ± 2 nm.

3.1.2. Convergence and angular correction. The effects of finite collection aperture and incident beam convergence angle influence the measured VEEL spectra. The single scattering distribution was corrected for these effects with the CONCOR routine of Egerton [10], which was modified to be applicable to the energy loss range from 0 to 100 eV and to include the angular correction necessary before Kramers Kronig analysis [10].

3.1.3. Kramers Kronig analysis. The single scattering distribution is proportional to $\mathrm{Im}(-1/\varepsilon)$ where ε is the dielectric function which depends on the energy and the momentum transfer. The latter is neglected here (see also discussion in section 4.3) and ε is taken to depend only on energy. The real part of this function was obtained by a FFT-based Kramers Kronig analysis [21]. Knowledge of $\mathrm{Im}(-1/\varepsilon)$ at all frequencies is required for KK analysis, but this is not available experimentally. Therefore the experimental data are extended using spectral wings. On the high-energy side the wing follows an analytical function A^*E^{-r} where E is the energy loss and r was set to 4. This function was matched to the experimental data in the energy loss region 50–54 eV and then extended up to 1000 eV. This procedure completely neglects the influence of the Al–L edge which occurs around 78 eV in α-Al_2O_3. For the low-energy losses wings are normally added, but since the energy loss goes to zero at the band-gap energy this was not necessary here. The resulting energy loss function should be on a quantitative scale, but will have an arbitrary scale because the incident electron beam intensity is not known accurately. Here the index sum rule [10] was used for absolute scaling with a refractive index of 1.767 at 633 nm determined for α-Al_2O_3 by optical spectroscopy.

3.1.4. Interband transition strength J_{CV}. From the real and imaginary parts of the dielectric function the complex interband transition strength is calculated [2]:

$$J_{CV}(E) = \frac{m_0^2}{e^2\hbar^2}\frac{E^2}{8\pi^2}\mathrm{i}\varepsilon^*(E) \qquad (1)$$

where m_0 is the mass of the electron, h is Planck's constant and E is the electron energy loss or photon energy. The asterisk denotes complex conjugation, so that the real part of the interband transition strength J_{CV} is proportional to the imaginary part of the dielectric function ε. For computational convenience we take the prefactor $m_0^2e^{-2}\hbar^{-2}$ whose value in cgs units is 8.289×10^{-6} g cm^{-3} eV^{-2} as set equal to one. Therefore the plotted J_{CV} spectra have units of eV^2. For the calculation of the sum rule (equation (2)) the prefactor has to be included and the units of J_{CV} are then g cm^{-3}. The intensity in the J_{CV} data obtained from VUV measurements goes to zero around 40 eV whereas the VEELS based J_{CV} has a non-zero intensity at this energy. This difference is not fully understood at the moment and might be due to the processing of either sets of data. In order to obtain comparable results, which are also suitable for further analysis, we have subtracted a linear baseline from the single scattering distribution which was constructed to touch the experimental data at 6 eV and 54 eV. The J_{CV} obtained in this way from the EELS is compared to the VUV results in figure 2(*b*).

3.1.5. Critical point modelling. The similarity in the interband transition strength for both methods indicates that the same critical point model as previously used for the VUV data [5] (figure 3(*a*)) can be fitted to the SR VEELS data. The models were optimized using maximum likelihood methods with simulated annealing [2].

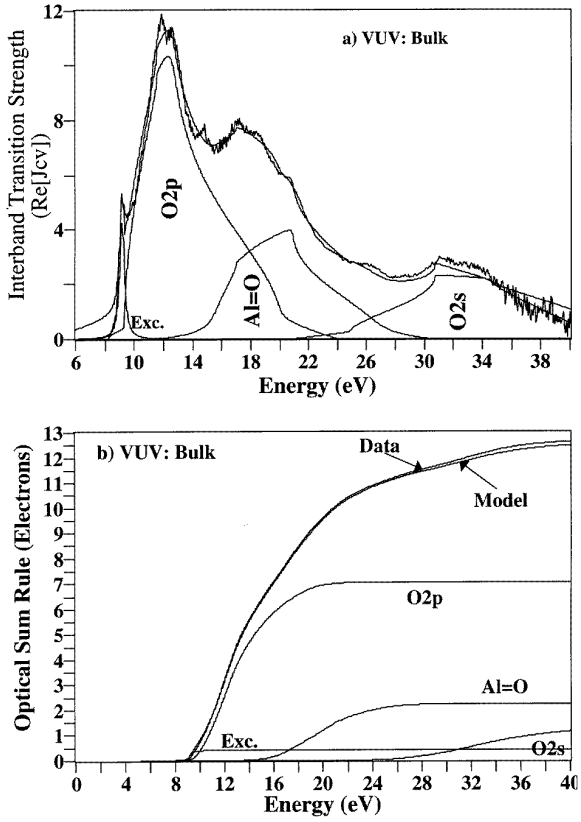

Figure 3. (*a*) Critical point models of the interband transitions from VUV data of α-Al_2O_3, and (*b*) partial optical sum rules for the critical point sets corresponding to interband transitions from the O 2p bands, Al=O hybridized bands and the O 2s lower valence bands to the Al conduction bands [5, 2]. An excitonic transition is resolved at the band gap in these VUV measurements.

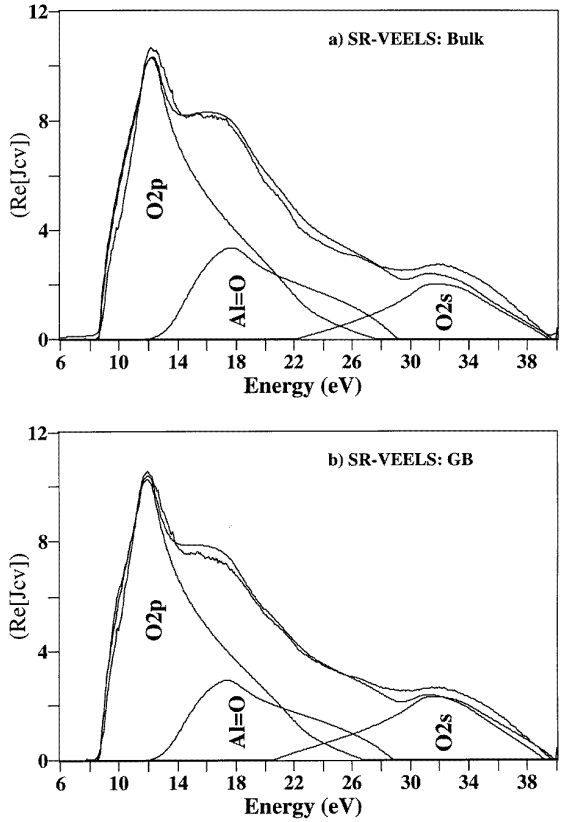

Figure 4. Critical point models of the interband transitions from STEM VEELS data of α-Al_2O_3, showing the critical point set corresponding to the interband transitions from the O 2p bands, Al=O hybridized bands and the O 2s lower valence bands to the Al conduction bands. The critical point models are fitted to (*a*) α-Al_2O_3 bulk grain and (*b*) the α-Al_2O_3 near-$\Sigma 11$ tilt grain boundary.

For α-Al_2O_3 it has been found that four sets of critical points appear, one exciton and three related to 3D sets of interband transitions. These correspond to the transitions from occupied valence bands into the unoccupied Al 3s and 3p conduction band. The valence bands in α-Al_2O_3 can be divided into three regions—the O 2s lower valence band and two upper valence bands. The latter comprises the O 2p band, which corresponds to the non-bonding electrons on oxygen arising from the charge transfer upon ionic bond formation, and below these lies the Al=O band with predominant hybridization of Al and O orbitals which is representative of covalent bonding. This interpretation of the upper valence band character is based on an analysis of the calculated band structure and site specific density of states (DOS) of α-Al_2O_3 which indicates that the O 2p has almost all its DOS on the O atoms, whereas the Al=O has roughly the same DOS on Al and O atoms [22]. The α-Al_2O_3 critical point model is shown in figure 3(*a*) refined onto the VUV derived J_{CV} spectra. In figure 4(*a*) the CP model fit is refined onto the bulk VEELS data and figure 4(*b*) shows the refined CP model for the GB VEELS data. Although only the real part of the interband transition strength is shown the model is fitted simultaneously to real and imaginary part (for details see [2]).

3.1.6. Oscillator strength sum rule. The oscillator strength or f-sum rule (equation (2)) can be used on the experimental data and on the individual balanced critical point sets to determine the valence electron density of the material and the electron occupancy of each CP set. The sum rule

$$n_{eff} = \frac{4m^* v_f}{m_0} \int_0^{h\nu} \frac{J_{CV}}{E}\,\mathrm{d}E \qquad (2)$$

where $m^* m_0$ is the effective mass of the electrons ($m^* = 1$ is taken in all calculations), v_f is the volume of the formula unit and J_{CV} is the interband transition strength, was applied to the model and the experimental data. The effective number of electrons n_{eff} is a dimensionless quantity which can easily be verified by combining equations (1) and (2). Figure 3(*b*) shows the partial sum rules for the VUV data while figure 5 compares the partial sum rules determined from the VEELS data. These results are summarized in table 1.

3.1.7. Ionicity. The upper valence band can be thought of as representing the character of the bonding. The ionicity of the bonding can be regarded as the number of electrons in the O 2p valence band with respect to the total number

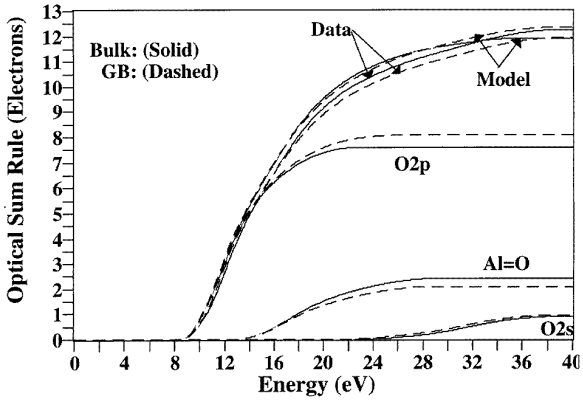

Figure 5. Partial optical sum rules of the interband transitions of α-Al_2O_3 fit to STEM VEEL spectra, showing electron occupancies for the critical point sets corresponding to the interband transitions from the O 2p band, Al=O hybridized band and the O 2s lower valence band to the Al conduction bands. Partial optical sum rules are compared for the α-Al_2O_3 bulk grain and the α-Al_2O_3 Σ11 grain boundary.

in the upper valence band. This yields 76% for the VEELS data in agreement with the VUV results [5].

3.2. Grain boundary

The spectra taken from the near-Σ11 grain boundary were processed and analysed in the same way as described for the bulk spectra above. The single scattering distribution (figure 2(*a*)) of the four spectra (2 GBs and 2 in bulk) show differences between the two sets. There are also some variations within each set, but they are smaller than the differences between the bulk and GB data sets. These differences in the VEEL spectra transform into differences in the interband transition strength (figure 2(*b*)). The critical point model is fitted (figure 4(*b*)) and the *f*-sum rule quantifies the differences (figure 5 and table 1). The main difference occurs in the energy region of the Al=O valence band transitions. The interband transition strength is reduced which leads to a smaller number of effective electrons in the Al=O covalent valence band. This translates into a higher ionicity of the atomic bonding in the GB region.

4. Discussion

4.1. Data comparison

4.1.1. VUV and VEEL spectroscopy. The interband transition strength obtained from the VEELS shows the same overall structure as the result from VUV spectroscopy. The energy resolution is less in the VEEL spectrum and therefore all features are less sharp and appear broadened. This is reflected in the critical point model in which the contributions from the different parts of the valence band show less structure. However, the only information which is lost is the sharp exciton peak which cannot be distinguished in the VEELS interband transition strength. The VUV results aided the development of the VEELS data analysis and the identification of artifacts resulting from incorrect data processing. The index sum rule used for scaling the measured energy-loss spectra requires an *a priori* knowledge, which will not be available for all materials, especially for unknown phases which are of interest. Another method is needed to achieve general applicability of the analysis without any *a priori* knowledge. The use of an erroneous value for the index of refraction in the index sum rule affects the interband transition strength strongest for low-energy losses [19]. Small errors in the correction for multiple scattering do not influence the interband transition strength strongly [19]. Although the multiple scattering correction makes crude approximations, the additionally introduced corrections are thought to render the remaining errors negligible. The subtraction of a linear baseline from the data to reduce the intensity around 40 eV to obtain an analysable result may be regarded as the largest approximation. The source of this baseline offset is currently not fully understood but with the improved analysis currently under development no corrections will be necessary. The analysis will be restricted to insulators with a band gap which is large enough to allow fitting in an energy-loss spectral region which is known not to have any intensity present. Alumina has a large band gap and is therefore a suitable material as are a number of other ceramic materials. Semiconductors and metals on the other hand will pose more severe problems.

Table 1. Effective number n_{eff} of electrons in the valence bands for α-Al_2O_3 calculated by the *f*-sum rule (equation (2)) from the experimental interband transition strength and the critical point model fitted to them. The interband transition strength was calculated from VUV reflectivity measurements of single crystal alumina [5], and VEELS for bulk α-Al_2O_3 and the near-Σ11 tilt grain boundary. The ionicity is taken as the ratio n_{eff} (O 2p)/(n_{eff}(O 2p) + n_{eff} (Al=O)). See text for further details. Al_2O_3 has 24 electrons per formula unit.

	VUV bulk	VEELS bulk	VEELS Σ11 GB
Experimental total	12.5	12.3	12.0
Model total	11.4	10.9	11.0
Exciton	0.9	—	—
O 2p	7.1	7.6	8.0
Al=O	2.2	2.4	2.1
O 2s	1.2	0.9	0.9
Ionicity	76%	76%	79%

It is well known that the *f*-sum rule hardly ever exceeds the valence electron count, and instead usually underestimates the electron density [23]. We therefore expect to find a total of about 24 electrons, whereas the experimental results show roughly half this number. (This result is in contrast to an earlier publication [3] which showed 24 valence electrons for alumina. However, in the course of the present study an error was found in the previous calculation yielding results twice as large.) This large discrepancy for alumina is currently being investigated further. The calculated partial sum rules contain an error, arising from the imperfect critical point

models. Currently there are no other results available for the exact number of electrons in the different parts of the valence band to check the consistency of our results. The ionicity as defined above is nevertheless meaningful and shows the general trend because it is a relative measure. The analysis method presented for VEEL spectra allows a detailed comparison with data obtained by optical spectroscopy and provides quantitative information about the optical properties and electronic structure of insulators.

4.1.2. Bulk material and grain boundary. The exact results for interband transition strength and f-sum rule depend on the details of the data analysis, which is a topic of ongoing development. In the present work on the near $\Sigma 11$ tilt grain boundary identical data analysis was applied to all data sets. It is reasonable to assume that the errors present in the analysis are systematic and therefore the differences in the original experimental data are translated into meaningful differences in the final result. The differences between the VEELS from the bulk material and the GB appear mostly in the energy-loss region starting at 14 eV and extending up to the plasmon energy (25 eV). This energy range corresponds to transitions from the covalent Al=O valence band into the Al 3p conduction band. The analysis shows that the corresponding interband transitions strength is reduced and the bonding is less covalent (more ionic) at the GB. While the absolute numbers given for the difference might not be reliable and depend on the details of the data analysis, the qualitative statement remains valid. In the course of this work we have performed the analysis on different data sets many times and we have changed practically all parameters. It was always found that the bonding at the interface is more ionic—the opposite was never observed.

4.2. Stability, energy resolution and counting statistics

The VEELS data are limited in two respects, one is the limited energy resolution and the other the statistics. The energy resolution of the experimental set-up is determined by several factors. The cold field emission source has an intrinsic width of 0.2 eV. This is broadened by instabilities in the microscope accelerating voltage and the resolution of the electron spectrometer. For this work the energy resolution of the whole system was 0.7 eV which is probably due to stray fields and imperfect spectrometer alignment. Similar systems have reported an energy resolution below 0.5 eV [24] and work is in progress to achieve this on the set-up used here.

The photodiode array has a limited dynamic range and a detective quantum efficiency which depends on the exposure [25]. For the quantitative analysis here it is important to measure not only the strong zero loss intensity accurately but also the inelastically scattered intensities; even those have a large dynamic range with the relatively strong plasmon and the weak intensities at the onset above the band gap. It is these relatively weak intensities and their shape which contain the most important information about the interband transition strength and which therefore have to be measured accurately. The variations observed between the two data sets from the bulk material are attributed to a combination of instabilities and the counting statistics. The variation in the two GB spectra could additionally be due to a variation in structure along the grain boundary [13, 14]. The variations between the two different data sets are more pronounced and therefore reflect differences between bulk and GB.

The dynamic range and noise characteristics of the photodiode have been slightly improved recently [26], but it remains essential to acquire spectra with different integration times and splice them to give one single spectrum as was done for this work. A newly developed computer-controlled system allows the acquisition of two spectra at the same location, one with a short integration time to obtain the zero loss peak and one with a long acquisition time for optimizing the plasmon region [27]. An additional advantage of this system is that the specimen is only exposed to the electron beam while data are acquired and electron beam irradiation damage is therefore restricted to the actual measurement.

4.3. Artifacts

In the retrieval of the interband transition strength from VEELS data several effects have to be kept in mind. Because of the difficulties of multiple scattering corrections, it is necessary to take VEELS data from thin specimens. The surfaces of the specimen contribute inelastic scattering which originates from the electrons traversing the solid/vacuum interface. The strength of the surface loss can be calculated if the dielectric function is known [10]. This property has to be determined by an iterative process, obtaining a first estimate of ε, then calculating the surface loss and subtracting it from the VEELS data, then reobtaining ε, etc. This was not included in the present analysis as the intensity of the surface loss for the specimen thickness investigated (80 nm) is negligible. However, an iterative scheme as described above could easily be implemented. More complicated is the case where the specimen is coated with a thin layer of another material. For insulators it is sometimes (but not in the present α-Al_2O_3 sample) necessary to coat the specimen with a thin carbon layer to avoid specimen charging during the investigation, since charging leads to unacceptable microscope instabilities. Sometimes contamination of the TEM specimen during electron beam irradiation occurs due to specimen contamination during preparation or insufficient vacuum in the microscope. Here the originally employed carbon coating was removed and contamination was not observed during the experiment. In cases where this is not possible it might be feasible to measure the thickness of the carbon layer by quantifying the carbon K-edge in an EEL spectrum and calculating the effect on the measured spectrum by assuming a dielectric function for carbon obtained in an independent experiment.

Electrons undergo some inelastic scattering processes which do not occur for photons. If the velocity of the primary electron beam is larger than the speed of light in the medium, Cherenkov radiation occurs [10]. Electrons accelerated to 100 keV have a velocity of $0.548 \times c$,

where c is the speed of light in vacuum. This means that Cherenkov radiation occurs in energy loss regions where the refractive index n is larger than 1.82 or ε is larger than 3.33. For alumina this condition is almost fulfilled for energies between 5 and 10 eV. For some other ceramic materials with higher values of ε this might be true for even larger spectral regions. Cherenkov radiation is strongly forward peaked. The cross section for this process, integrated over scattering angle, is small compared to other processes. This argument also applies to surface guided modes, which have been observed in amorphous alumina [28]. Since the VEELS spectra here were acquired integrating over scattering angle the contributions from Cherenkov radiation and surface guided modes have been neglected. A Cherenkov correction can be developed using the same iterative approach as discussed for surface losses, since its strength can be given analytically.

The inelastic scattering of electrons involves a momentum transfer. For 100 keV electrons the wavelength is 3.7 pm and the wavevector $k_0 = 1697$ nm^{-1}. The characteristic scattering angle θ_E for inelastic scattering for an energy loss of 20 eV is 0.1 mrad and therefore much smaller than the scattering angle θ allowed by the apertures. The momentum transfer $q^2 = k_0^2(\theta_E^2 + \theta^2)$ can then be approximated as $q = k_0\theta$ which amounts to 11.9 nm^{-1}. The optical limit is $q = 0$. Electron scattering experiments, however, often use $q = 2$ nm^{-1} to avoid the influence of surface effects and Cherenkov radiation. In this paper we work in the approximation $\varepsilon(q, E) = \varepsilon(E)$ which is typically used in the analysis of data obtained with transmission electron microscopes. Because we require spatial resolution in our experiments and the acquisition times have to be short, it is not possible to work with the small apertures sometimes used with dedicated electron scattering aparatus without spatial resolution. As can be seen from our results this approximation is valid in the case of α-Al_2O_3. This can be explained from band structure calculations for α-Al_2O_3 [22] which show that the bands are flat over large regions and therefore the band dispersion is small. For other materials it is found that a momentum transfer of 10 nm^{-1} significantly changes the shape of the dielectric function [29].

Electrons also scatter inelastically with phonons. These energy losses are of the order of a few tens of millielectronvolts and can therefore not be resolved with transmission EEL spectroscopy in an electron microscope. These quasi-elastic scattering processes broaden the zero-loss peak on the high-energy side. Since they do not contain information about the interband transitions it is desirable to remove them from the measured spectra. This is achieved automatically by fitting the zero-loss line shape assuming zero intensity in the band-gap region. However, it is not clear which shape the phonon scattering process contributes at higher energy losses leading to an uncertainty in whether it has been removed properly. This might explain some of the discrepancies observed between data from VEEL and VUV spectroscopy.

4.4. Spatially resolved information

In the past the analysis of VEELS has been limited to bulk materials [29, 30] or special geometries [12]. In the latter case dielectric theory has been used to evaluate the detailed influence of the geometry on the recorded VEEL spectrum [12]. For example, the presence of internal interfaces or of holes in a specimen of cylindrical geometry may give rise to prominent interface plasmons when the properties of the materials are appropriate [31]. For a known geometry such as a planar interface between two media it is possible to calculate the observed VEELS as a function of the electron probe distance from the interface using the dielectric functions of the two materials [31]. In these cases, for particular values of the material's dielectric constants, interface plasmons may appear due to the geometry of the sample and not due to any dielectric properties unique to the interface itself. This suggests that it is not always possible to interpret the VEELS data locally, but that they can depend on the environment surrounding the electron beam. Therefore the analysis of such VEELS data would have to proceed in a similar way to the possibility indicated above for the correction of surface effects. First the dielectric function of the two bulk materials has to be determined and then the expected VEELS calculated. The comparison of this with the spatially resolved measurement should then reveal any influence of the interface and the bonding present on the dielectric function.

In the analysis of the energy-loss near-edge structures (ELNES) of inner shell ionization edges in the EEL spectra it has been assumed that the ELNES of all irradiated atoms adds up linearly. Therefore it is possible to extract the interfacial ELNES by the spatial difference method [32], a subtraction of the reference signal obtained in bulk material near the interface. Here this is not possible because of the complex nature of the low energy-loss signal. Due to the averaging by rastering the beam over an area of 3 nm $\times$ 4 nm the measured VEELS contains information from the bulk material, the GB and also the geometry of them in the specimen. The inelastic scattering process itself at these low energy losses of the primary electrons is not well localized [33] due to the uncertainty principle. It is not clear how local the information would be even if an electron beam with the smallest possible diameter (here 0.22 nm) were used.

In the case of a grain boundary, i.e. a homophase boundary, the situation is somewhat different. It is possible to regard the interface as a layer of a thickness (which in the case of atomically abrupt interfaces would be of the order of interatomic distances) which has a dielectric function ε_I which differs from the bulk dielectric function ε_B. This would be the case of a sandwich structure for which the VEELS can be calculated as a function of electron probe position from dielectric theory (analogous to the simple interface case). We have not employed any correction for this geometry so far, although we may in the future. The assumption and approximation made in this paper is that the change in the dielectric function is small at the interface. This is experimentally immediately obvious since no strong features appear in the interface spectrum. The

Kramers Kronig analysis is possible and does not present any approximation because its foundation is the causality principle which is obeyed. However, the determined functions are $\mathrm{Im}(-1/\varepsilon)$ and $\mathrm{Re}(-1/\varepsilon)$ where ε is now an *effective* dielectric function. Prescriptions have been given for constructing such effective dielectric constants for various cases, such as Maxwell–Garnett theory and extensions by Howie and Walsh [34]. The determination of ε from these functions is not easy and has not been attempted here. Rather it is assumed that this interfacial region has an effective dielectric function ε which is then used in all following analyses. This will lead to an effective interband transition strength and a critical point model of it. The results given for the $\Sigma 11$ grain boundary describe these effective properties of the interfacial region. The result depends on the size of the rastered area and it is therefore not independent of the experiment. This limitation will be made smaller in the future by recording with the smallest beam diameter possible. Also, more sophisticated analysis procedures should be able to yield the interfacial ε independent of the measurement procedure and for all possible interfaces. This remains the aim in the long term of the work presented here but, at present, despite the necessary approximations, the analysis shows that it is possible to obtain information on the influence of the interface on the dielectric function ε and determine changes in the interfacial bonding. The absolute numbers given are probably not correct at the time being, but the trend is reliable.

4.5. Comparison to other studies

As mentioned in the introduction this particular near-$\Sigma 11$ tilt grain boundary in α-Al_2O_3 has been studied by a number of techniques and methods. HRTEM [13] has shown an atomically abrupt interface with periodic structures along the grain boundary. The quantitative comparison of the experimental images with image simulations for a structure obtained by static lattice calculations has given good agreement [14]. These calculations have found that this GB has a low energy and that the same structure is obtained independently of the potential used in the calculations. The interfacial ELNES has been obtained by the spatial difference method [15]. A detailed analysis has shown that the interfacial Al atoms have a coordination to their neighbouring O atoms which is reduced from the six-fold coordination present in bulk α-Al_2O_3. The bond length increases and shows a larger distribution than in the bulk material. A quantitative analysis has shown that one monolayer of Al atoms is affected by the presence of the interface. All these findings have been obtained by the self-contained analysis of the ELNES data [15]. A comparison to the atomic position from the calculated structure showed good agreement with all these statements.

More recently there has been a first principles calculation of the electronic structure [16] and the optical properties [17] based on the structural model [14]. The density of states with p-symmetry in the conduction band agrees well with the experimental ELNES. A charge transfer was found from the Al to the O atoms at the interface. This means that the bonding there is more ionic—in agreement with the results presented here.

The near-$\Sigma 11$ tilt grain boundary in α-Al_2O_3 has been investigated by all these techniques and many results have been obtained independently by two different techniques. Because of the consistency of all the evidence available we believe that the atomistic and electronic structure of this particular GB is now understood. This has of course been a model study, developing techniques. Because of its success many of the methods are now employed for investigations of other interfaces. We also believe that the analysis of VEELS and determination of the electronic structure and bonding from it will be successfully applied to other systems. First, other grain boundaries in α-Al_2O_3 will be investigated, for example a twin boundary with and without Ca segregation which has already been studied by HRTEM [35]. General high-angle GBs without impurities should show a stronger effect since the GB energy is larger and therefore more pronounced changes in the electronic structure are expected.

4.6. Future work

In the future the analysis will be developed further in order to take some of the effects into account which have been neglected so far (see discussion above). In particular a case study of the spatial information present in the VEELS and an iterative calculation of the dielectric function considering the geometry will be attempted. First attempts have been made by recording VEELS data across the $\Sigma 11$ GB and acquiring spectra with a nominal spacing of 0.1 nm. So far the statistics in the data are not sufficient to analyse them reliably. Modern methods of data analysis such as artificial neural networks [36] might be useful for classification of these large data sets and could reduce the detailed analysis and modelling to a few standard spectra. Alternatives to the index sum rule scaling and the subtraction of a linear baseline will be sought to make the data analysis independent of *a priori* knowledge.

5. Conclusions

Quantitative determination of the interband transition strength and the electronic structure from an analysis of VEELS yields comparable results to the more established VUV spectroscopy results. For the spatially resolved analysis of a near-$\Sigma 11$ tilt grain boundary in α-Al_2O_3 the differences in the VEELS translate into differences in the interband transition strength. From critical point modelling of the interband transition strength the bonding at this internal interface is more ionic with respect to bulk α-Al_2O_3. This result is in good agreement with other experimental and theoretical investigations of the same GB. The VEELS data analysis is complex and this is believed not to influence the qualitative results, though it may have an influence on the quantitative result. Much work remains to be done but the results presented here are very encouraging. VEELS analysis represents a new method to determine dielectric properties, electronic structure and bonding with high spatial resolution.

Acknowledgments

We thank Dr P A Morris for fabricating the bicrystal, Dr T Höche for preparing the cross sectional TEM specimen, Dr S Loughin for critical point analysis, Dipl. Phys. G Duscher and Dr L K DeNoyer for software development and Professor M Rühle and Dipl. Phys. A Pfleiderer for useful discussions. We are grateful to Professor W Y Ching for making the results of his calculations available prior to publication.

References

[1] Wooten F 1972 (New York: Academic)
[2] Loughin S, French R H, DeNoyer L K, Ching W-Y and Xu Y-N 1996 Critical point analysis of the interband transition strength of electrons *J. Phys. D: Appl. Phys.* **29** 1740
[3] French R H 1990 Electronic structure of α-Al_2O_3, with comparison to AlON and AlN *J. Am. Ceram. Soc.* **73** 477–89
[4] Bortz M L, French R H, Jones D J, Kasowski R V and Ohuchi F S 1990 Temperature dependence of the electronic structure of Al_2O_3, $MgAl_2O_4$ and MgO *Phys. Scr.* **41** 537–41
[5] French R H, Jones D J and Loughin S 1994 Interband electronic structure of α-Al_2O_3 up to 2167 K *J. Am. Ceram. Soc.* **77** 412–22
[6] Loughin S, French R H, Ching W Y, Xu Y N and Slack G A 1993 Electronic structure of aluminum nitride: theory and experiment *Appl. Phys. Lett.* **63** 1182–4
[7] Loughin S and French R H 1994 Optical functions of aluminum nitride *Properties of Group III Nitrides* ed J H Edgar (London: INSPEC) pp 175–89
[8] French R H, Cannon R M, DeNoyer L K and Chiang Y-M 1995 Full spectral calculation of non-retarded Hamaker constants for ceramic systems from interband transition strengths *Solid State Ionics* **75** 13–33
[9] French R H, Scheu C, Duscher G, Müllejans H, Hoffmann M J and Cannon R M 1995 Interfacial electronic structure and full spectral Hamaker constants of Si_3N_4 intergranular films from VUV and SR-VEEL spectroscopy *Materials Research Society Symp. Proc. 357* ed D Bonnell, U Chowdhry and M Rühle, pp 243–8
[10] Egerton R F 1986 *Electron Energy-Loss Spectroscopy in the Electron Microscope* (New York: Plenum)
[11] Walls M G 1987 Electron energy-loss spectroscopy of surfaces and interfaces *PhD Thesis* University of Cambridge, UK
[12] Walsh C A 1989 Modelling and interpretation of electron energy-loss spectra from interfaces *PhD Thesis* University of Cambridge, UK
[13] Höche T, Kenway P R, Kleebe H-J, Rühle M and Morris P A 1994 High resolution transmission electron microscopy studies of a near-Σ11 grain boundary in α-alumina *J. Am. Ceram. Soc.* **77** 339–48
[14] Kenway P R 1994 Calculated structures and energies of grain boundaries in α-Al_2O_3 *J. Am. Ceram. Soc.* **77** 349–55
[15] Bruley J 1993 Spatially resolved electron energy-loss near-edge structure analysis of a near-Σ11 tilt boundary in sapphire *Microsc. Mircoanal. Microstruct.* **4** 23–39
[16] Mo S-D, Ching W Y and French R H 1996 Electronic structure of a near-Σ11 α-axis tilt grain boundary in α-Al_2O_3 *J. Am. Ceram. Soc.* **79** 627–33
[17] Mo S-D, Ching W Y and French R H 1996 Optical properties of a near-Σ11 α-axis tilt grain boundary in α-Al_2O_3 *J. Phys. D: Appl. Phys.* **29** 1761
[18] Müllejans H, Bruley J, French R H and Morris P A 1993 Quantitative electronic structure analysis of α-Al_2O_3 using spatially resolved valence energy-loss spectra *Proc. Electron Microscopy and Analysis Group (EMAG) of Royal Microscopical Society* ed A J Craven (Bristol: IOP Publishing) pp 59–62
[19] Müllejans H, Bruley J, French R H and Morris P A 1994 Quantitative electronic structure analysis of α-Al_2O_3 using spatially resolved valence electron energy-loss spectra *Materials Research Society Proc. Symp. 332* ed M Sarikaya, K Wickramasighe and M Isaacson, pp 169–76
[20] Morris P A 1986 High purity Al_2O_3: processing and grain boundary structures *PhD thesis* Massachusetts Institute of Technology, Cambridge, MA, USA
[21] Bortz M L and French R H 1989 Quantitative, FFT-based, Kramers Kronig analysis for reflectance data *Appl. Spectrosc.* **43** 1498–1501
[22] Xu Y-N and Ching W Y 1991 Self-consistent band structures, charge distributions, and optical-absorption spectra in MgO, α-Al_2O_3 and $MgAl_2O_4$ *Phys. Rev.* B **43** 4461–72
[23] Smith D Y 1985 Dispersion theory, sum rules, and their application to the analysis of optical data *Handbook of Optical Constants of Solids* ed E D Palik (New York: Academic) pp 35–68
[24] Batson P E, Johnson D W and Spence J C H 1992 Resolution enhancement by deconvolution using a field emission source in electron energy loss spectroscopy *Ultramicrosc.* **41** 137–45
[25] Krivanek O L, Ahn C C and Keeney R B 1987 Parallel detection electron spectrometer using quadrupole lenses *Ultramicrosc.* **22** 103–16
[26] Tencé N 1994 *Proc. 32nd Colloquium of the French Society of Electron Microscopy (Rouen, 1992)* as cited in Colliex C, Tencé M, Lefèvre E, Mory C, Gu H, Bouchet D and Jeanguillaume C 1994 Electron energy loss spectrometry mapping *Mikrochim. Acta* **114–115** 71–87
[27] Duscher G and Thomas J 1995 private communication
[28] Chen C H and Silcox J 1975 Surface guided modes in an alumina oxide thin film *Solid State Commun.* **17** 273–5
[29] Fink J 1989 Recent developments in energy-loss spectroscopy *Adv. Electronics Electron Phys.* **75** 121–232
[30] Livins P, Aton T and Schnatterly S E 1988 Inelastic electron scattering in amorphous silicon nitride and aluminium oxide with multiple-scattering corrections *Phys. Rev.* B **38** 5511–19
[31] Howie A and Milne R H 1985 Excitations at interfaces and small particles *Ultramicrosc.* **18** 427–34
[32] Müllejans H and Bruley J 1995 Electron energy-loss near-edge structure of internal interfaces by spatial difference spectroscopy *J. Microsc.* **180** 12–21
[33] Howie A 1981 Localization and momentum transfer in inelastic scattering *Proc. 39th EMSA* ed G W Bailey (San Francisco: San Francisco Press) pp 186–9
[34] Howie A and Walsh C A 1991 Interpretation of valence loss spectra from composite media *Microsc. Microanal. Microstruct.* **2** 171–81
[35] Höche T 1994 Hochauflösungselektronenmikroskopische Untersuchungen zur atomistischen Struktur von Korngrenzen in α-Al_2O_3 *PhD Thesis* Universität Stuttgart, Germany
[36] Gatts C, Duscher G, Müllejans H and Rühle M 1995 Analysing line scan EELS data with neural pattern recognition *Ultramicrosc.* **59** 229–39